

Article

Effects of Water and Cyclic Loading on Ultrasonic and Mechanical Properties of Sandstone: An Experimental Study

Yan Chen ^{1,2}, Guolong Zhang ¹, Erhu Bai ^{1,2}, Baohua Guo ¹ and Rong Dou ^{1,*}¹ School of Energy Science and Engineering, Henan Polytechnic University, Jiaozuo 454000, China² Collaborative Innovation Center of Coal Work Safety and Clean High Efficiency Utilization, Henan Polytechnic University, Jiaozuo 454000, China

* Correspondence: dourong@hpu.edu.cn

Abstract: In this study, the water absorption, mechanical properties, and energy evolution characteristics of sandstone were examined through experimental and theoretical analysis. The P-wave velocity was found to initially decrease, then increased with immersion time and water content. The water absorption rates of three sandstone specimens decreased with immersion time and water content. The post-peak deformation of the sandstone changed from brittle failure to strain softening. With the increase in water content, the peak strength and loading Young's modulus per cycle decreased. The loading Young's modulus showed that the unloading stress and increment of unloading stress nonlinearly increased with the number of cycles and decreased before peak strength. With the increase in the number of cycles, residual strains of the sandstone specimens decreased slightly initially and then increased, while the elastic strains increased before peak strength and then decreased at the post-peak stage. With the increase in unloading stress, the energy densities nonlinearly increased. At the same unloading stress, an increase in water content led to an increase in the input energy density and energy ratios of the sandstone specimens.



Citation: Chen, Y.; Zhang, G.; Bai, E.; Guo, B.; Dou, R. Effects of Water and Cyclic Loading on Ultrasonic and Mechanical Properties of Sandstone: An Experimental Study. *Energies* **2022**, *15*, 7908. <https://doi.org/10.3390/en15217908>

Academic Editors: Chun Zhu, Zhigang Tao, Xiaojie Yang, Fei Wu and Xiaoshuang Li

Received: 28 July 2022

Accepted: 21 October 2022

Published: 25 October 2022

Publisher's Note: MDPI stays neutral with regard to jurisdictional claims in published maps and institutional affiliations.



Copyright: © 2022 by the authors. Licensee MDPI, Basel, Switzerland. This article is an open access article distributed under the terms and conditions of the Creative Commons Attribution (CC BY) license (<https://creativecommons.org/licenses/by/4.0/>).

Keywords: water content; P-wave velocity; strength; young's modulus; residual strain; energy density

1. Introduction

Due to the effects of blasting and excavation, rock masses are often subjected to cyclic loading and unloading compression. In mining engineering, rocks often experience extreme and complex conditions including high ground stress and high karst water pressure, which can lead to rock burst, coal bump, roof fall, and water inrush due to the coalescence of fractures and energy release [1–4]. In China, water inrush is one of the most serious hazards which affect the safety of the workers and the production of coal in mining engineering [5]. Due to the effects of water and mining-induced stress, the rocks may suffer failure which results in water inrush and threaten the safety of workers. Therefore, it is necessary to understand the deformation failure characteristics and energy evolution law of rocks containing water under cyclic loading and unloading compression.

Sandstone, as a sedimentary rock, is widely encountered in rock engineering, such as tunnel engineering, dam-based engineering, slope engineering, and mining engineering [6–9]. Most previous laboratory studies have focused on the mechanical behaviors of sandstone under cyclic and monotonic loading [10–13]. Ray et al. [14] examined the effect of cyclic loading on the mechanical behavior of sandstone and found that the percentage decrease in uniaxial compressive strength (UCS) increased with the number of cycles. Gatelier et al. [10] investigated the mechanical properties of porous sandstone and two inelastic mechanisms (compaction and microcracking) were discussed. Fuenkajorn and Phueakphum [15] presented the experimental results of the compressive strength of rock salt. Their results showed that compressive strength decreased with increasing the number of loading cycles. In the aspect of the effects of water on the mechanical properties of rocks,

Baud et al. [16] investigated the weakening effects of water on sandstone and found that the reductions of brittle strength in the presence of water ranged from 5% to 17%. Using the published data, Vásárhelyi and Ván [17] presented a method to estimate the effects of water content on sandstone rock. Erguler and Ulusay [18] conducted laboratory tests to quantify the effects of water content on the mechanical properties of the rocks. Their results showed that with increasing water content, the uniaxial compressive strength and elastic modulus were reduced up to 90% and 93%, respectively. Li et al. [19] investigated the effects of water content on the strength of sedimentary rocks by triaxial compressive tests and showed that the reduction of strength by water content was related to a reduction in friction angle.

These researchers investigated the effects of water content on the mechanical properties of rocks by uniaxial and triaxial monotonic compression. However, the effects of water on the ultrasonic properties, such as deformation and energy evolution characteristics, of rocks under cyclic loading and unloading compression state should be paid more attention to. The sandstone used in this study was collected from the roof of a mining roadway in the Beizao coal mine, Shandong Province, China. The Beizao coal mine is adjacent to the Bohai Sea, and the main mining region is underneath the sea. The amount of water in the mining area is large and the sandstone significantly swells and softens when encountering the water; these conditions make it difficult to support and maintain the roadway. Therefore, it is necessary to study the mechanical properties of the Beizao sandstone with different water content in the Beizao coal mine.

In this paper, we report the results of a series of uniaxial monotonic and cyclic compression tests on sandstone with different water content. Based on the water absorption property of the sandstone, the relationship between P-wave velocity and water content is first presented. Using the experimental results of the sandstone under cyclic loading, the influence of the number of cycles and water content on the strength and deformation were analyzed. Finally, the energy evolution characteristics of the sandstone with various water content were evaluated.

2. Laboratory Testing

2.1. Sample Preparation

The sandstone examined was sedimentary rock and had an average unit weight of approximately 2.31 g/cm^{-3} . The X-ray diffraction (XRD) tests results are shown in Figure 1. In this test, all the samples were cored from sandstone blocks to an actual diameter of 50 mm and approximate 100 mm in length which per the standards of the International Society for Rock Mechanics and Engineering (ISRM) suggested specification [20]. All the tests were performed at a room temperature of approximately $25 \text{ }^{\circ}\text{C}$. Table 1 lists the physical properties of Beizao sandstone samples and the loading scheme for each specimen in this study.

Table 1. Physical parameters of tested sandstone specimens and loading scheme in this study. *D* and *L* represent diameter and length, respectively; *m* is rock mass and ρ is density.

| Sample | D (mm) | L (mm) | m (g) | ρ (g/cm^{-3}) | Immersion Time (min) | Loading Scheme |
|--------|--------|--------|--------|-------------------------------|----------------------|----------------------------|
| UC-S-1 | 49.36 | 99.34 | 440.88 | 2.319 | 0 | Uniaxial monotonic loading |
| UC-C-1 | 49.35 | 99.80 | 440.10 | 2.305 | 0 | Uniaxial cyclic loading |
| UC-W-2 | 49.45 | 99.70 | 443.15 | 2.314 | 260 | Uniaxial cyclic loading |
| UC-W-3 | 49.59 | 100.64 | 449.51 | 2.312 | 1300 | Uniaxial cyclic loading |
| UC-W-4 | 49.55 | 100.89 | 447.63 | 2.301 | 1800 | Uniaxial cyclic loading |

2.2. Water Content and P Wave Velocity Measurement

Before immersion into the water, the sandstone specimens were dried until the mass did not change and then the dry mass was measured. After measuring the dry mass, the test samples were immersed in water in a vacuum device shown in Figure 2a. The wet mass of each sample was then measured by electronic scale after the immersion before the test.

After measuring the wet mass, the P–wave velocity was measured by a circumferential velocity anisotropy apparatus. Figure 2b shows the Geotechnical Consulting & Testing Systems. The end surfaces of the samples were painted with grease as a coupling agent to make the transit time more accurate.

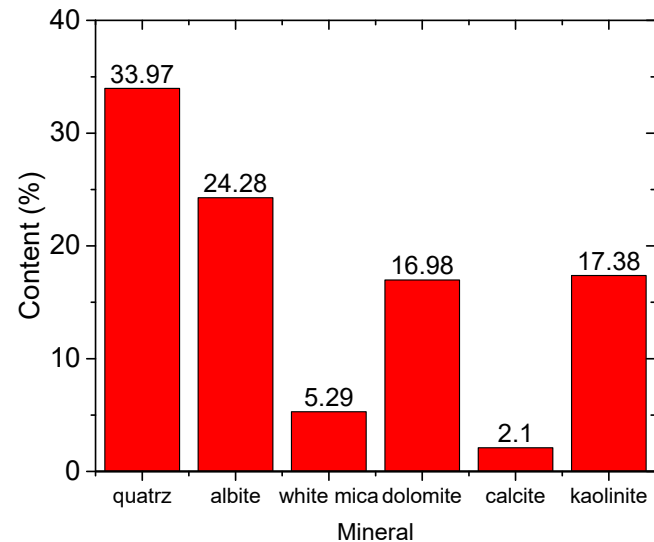


Figure 1. The mineral composition and content of Beizao sandstone.

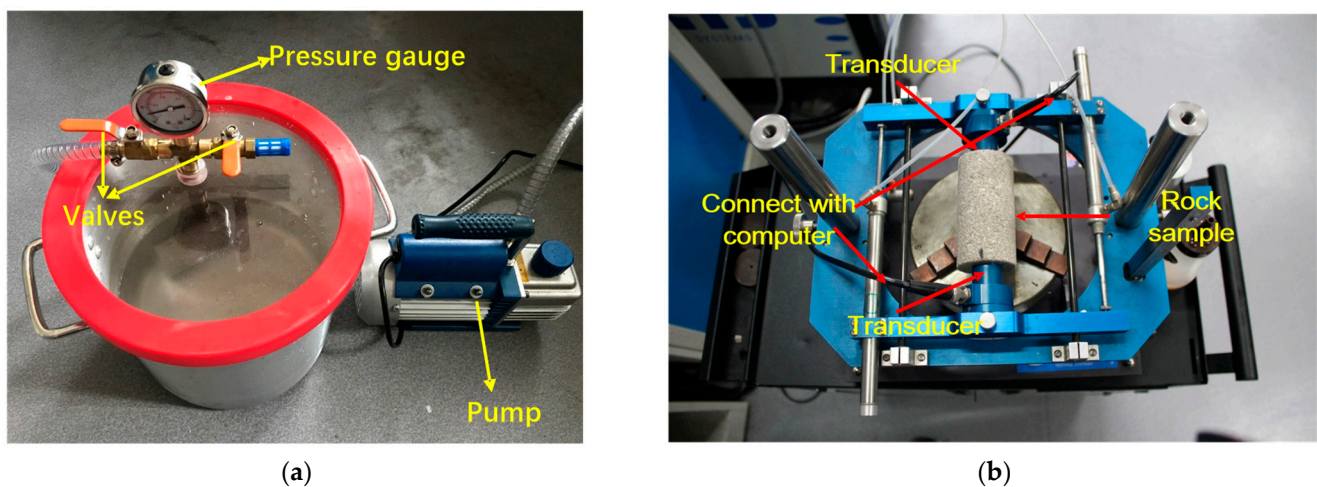


Figure 2. Experimental measurement: (a) vacuum device and (b) circumferential velocity anisotropy apparatus.

2.3. Experimental Setup

As shown in Figure 3, the mechanical behaviors of the sandstone were tested on a stiff servo-controlled testing machine (GCTS RTR–1000). The GCTS RTR–1000 has an axial load capacity of 1500 kN and a frame stiffness of 10 GN/m. The testing machine is equipped with a triaxial confining pressure cell of 140 MPa and linear variable differential transformers (LVDTs) for axial and circumferential strain measurements. A transparent thermoplastic membrane was wrapped around the specimen in both uniaxial and triaxial compression tests. The two axial extensometers on the sides of the specimen, fixed on the black rings, are the axial strain LVDTs, and the central rim is the radial strain LVDT.

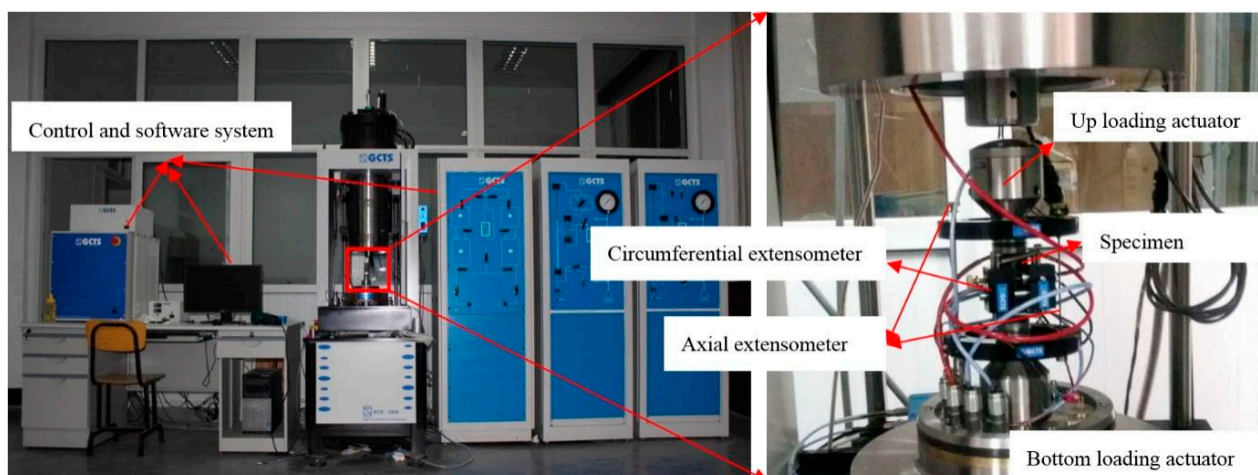


Figure 3. Illustration of the GCTS RTR-1000 testing system. The (right) photograph is the enlarged drawing of the red frame in (left) photograph [21,22].

To investigate the deformation failure characteristics of Beizao sandstone containing different water content, we performed two types of uniaxial tests: a monotonic compressive test, and a cyclic loading and unloading test. The uniaxial monotonic test was carried out under axial strain control at a loading strain rate of 0.02% per min until the failure of the sample. In the uniaxial cyclic tests, because the loading rates have different effects on the mechanical properties of rocks [23–25], loading and unloading rates were kept at a controlled axial strain rate of 0.02% per min, the same as in uniaxial monotonic tests. Each sample was continuously loaded and unloaded with the interval strain of 0.03%, which can be expressed as the following: $0 \rightarrow 0.03\% \rightarrow 0 \rightarrow 0.06\% \rightarrow 0 \rightarrow 0.09\% \dots 0.45\% \rightarrow 0 \rightarrow 0.48\% \rightarrow 0 \rightarrow 0.51\% \dots$. Then the samples were subsequently compressed until failure occurred at a loading rate of 0.02% per min.

3. Experimental Results of Beizao Sandstone under Cyclic Loading

3.1. Water Absorption Property

The water content of each sample was calculated by the mass difference between wet and dry mass divided by its dry mass, which can be expressed as:

$$w = \frac{\Delta m}{m_{(dry)}} = \frac{m_{(wet)} - m_{(dry)}}{m_{(dry)}} \quad (1)$$

where w is water content; $m_{(wet)}$ is the wet mass; $m_{(dry)}$ is the dry mass, and Δm is the mass difference between wet mass and dry mass.

Two parameters, increasing rate of mass of the sample (k_w) and increasing rate of the water content of the sample (v_w) were proposed to show the kinetics of the water adsorption in the sandstones. They can be calculated by the following equations below:

$$k_w = \frac{m_{i+1} - m_i}{t_{i+1} - t_i} \quad (2)$$

$$v_w = \frac{w_{i+1} - w_i}{t_{i+1} - t_i} \quad (3)$$

where i is the measuring number which is equal to 0, 1, 2 ... ; m_{i+1} and m_i are the masses of the sample at the measuring number of $i + 1$ and i , respectively; w_{i+1} and w_i are the water contents at the measuring number of $i + 1$ and i , respectively; t_{i+1} and t_i are the measuring time at the measuring number of $i + 1$ and i , respectively.

The final water contents of each sample were 2.992% (UC-W-2), 3.493% (UC-W-3), and 3.936% (UC-W-4). Figure 4 shows the relationship between mass difference, water

content, and immersion time. It can be observed from Figure 4 that both mass difference and water content exhibit similar trends with increasing immersion time. The rate of increase, including k_w and v_w , are shown in Figure 4c,d. One can observe from Figure 4c,d that both k_w and v_w decreased with immersion time, which indicates that the water absorption ability of Beizao sandstone decreases with an increase in immersion time.

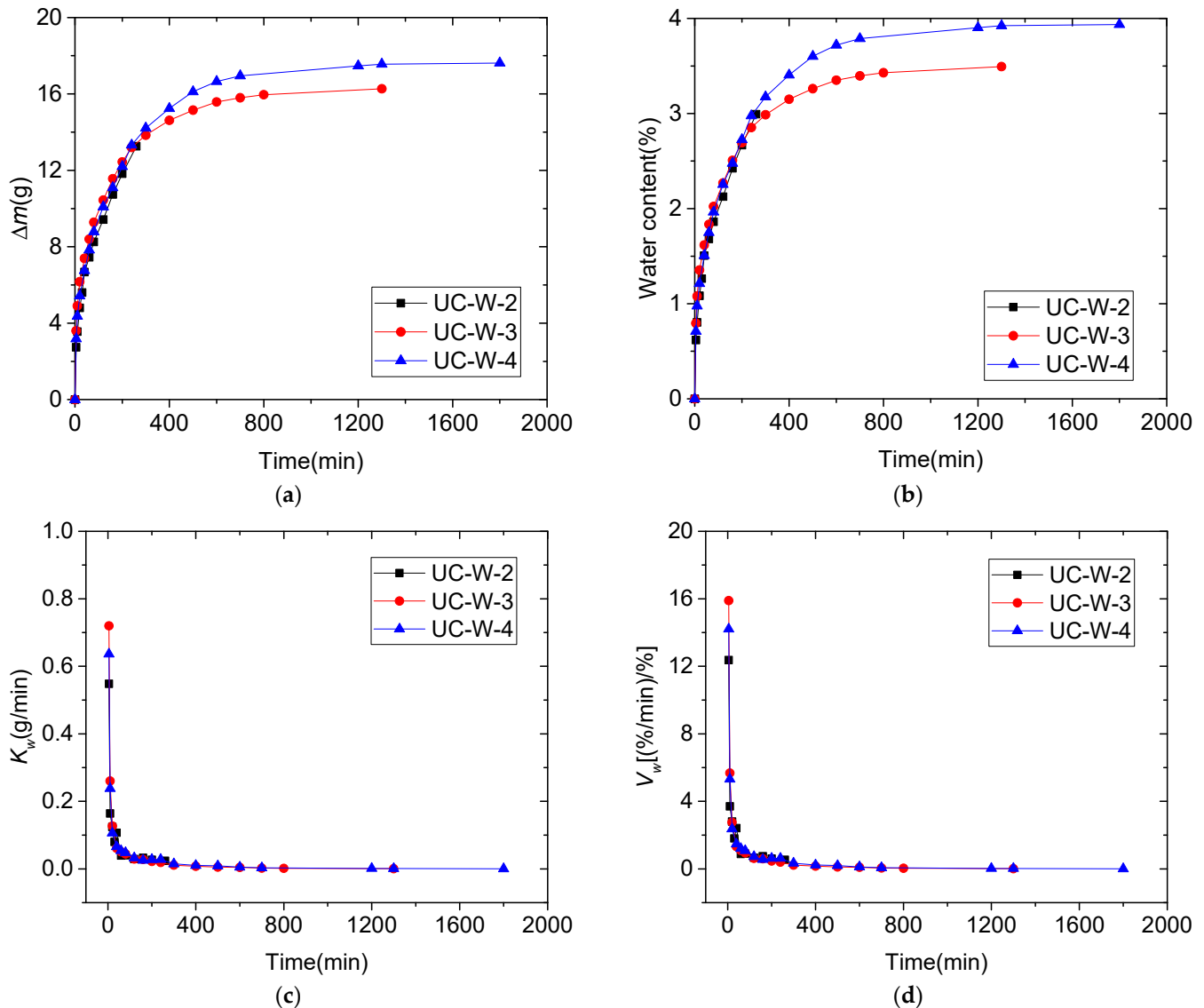


Figure 4. Variations of mass difference and water content (k_w and v_w , respectively) with immersion time: (a) the relationship between Δm and immersion time, (b) the relationship between w and immersion time, (c) the relationship between k_w and immersion time, (d) the relationship between v_w and immersion time.

3.2. P-Wave Velocity Evolution with Water Content

The variation of P-wave velocity with immersion time and water content was investigated on the Beizao sandstone. The plots of P-wave velocity with immersion time and water content are shown in Figure 5. It can be observed from Figure 5a that the P-wave velocity of all samples (UC-W-2, UC-W-3, UC-W-4) initially decreased sharply, and then gradually increased with the increase of immersion time. The turning points in immersion time between the decrease and increase of the P-wave velocity of Beizao sandstone specimens were approximately 200 (UC-W-2), 300 (UC-W-3), and 240 min (UC-W-4). Also, the evolution of the P-wave velocity with the water content in Figure 5b showed a similar trend to Figure 5a. At the water content of approximately 2.667% (UC-W-2),

2.986% (UC-W-3), and 2.975% (UC-W-4), the P-wave velocity started increasing with the increase in water content.

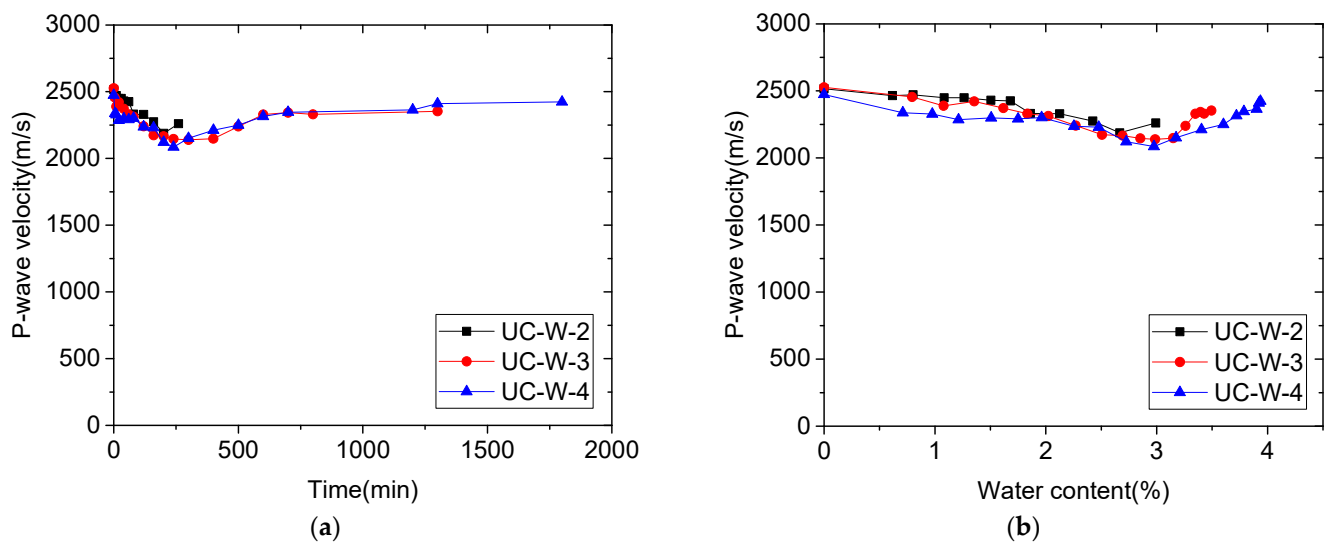


Figure 5. Variations of mean P-wave velocity with immersion time and water content: (a) relationship between P-wave velocity and immersion time and (b) relationship between P-wave velocity and water content.

Earlier studies [26–29] have investigated the effect of water content and saturation time on the P-wave velocity of rocks and found the P-wave velocity to increase with the water content and saturation time. Karakul and Ulusay [30] investigated the P-wave velocity of various rocks and observed both increase and decrease tendencies in P-wave velocity depending on the degree of saturation. In our experiments, there are two influencing factors explaining the reason why the P-wave velocity initially decreased and then increased. The first factor is that the water changed the microstructure of the sandstone specimens after immersion into the water, i.e., the inclusions or clay minerals dissolve and the matrix becomes loose. This factor results in the decrease in P-wave velocity. The other factor is mainly related to water itself, which is positive to the P-wave velocity. As we all know, the P-wave velocity in water is faster than it is in the air. After immersion into the water, with the increase in water content, the P-wave velocity increases. The two factors influence the P-wave velocity together. With the increase in water content, the effects of the first factor will gradually decrease, and the effects of water will strengthen. The illustration can be seen in Figure 6.

3.3. Stress-Strain Curves

Figure 7 shows the stress-strain curves for the Beizao sandstone under uniaxial cyclic loading and unloading compression. Results showed similar characteristics to the earlier studies [31–35]. In phase I, the crack closure phase, the stress-strain curve displayed an initial nonlinear phase due to the closure of the micro cracks. In phase II, the elastic phase, the rock matrix underwent elastic deformation. Phase III is the crack stable growth phase; this is where the micro-cracks started initiating and propagating due to the stress concentration at the tip of micro cracks with the increasing axial load. Phase IV represents the unstable crack growth stage until the stress reached the peak value. Phase V is the post-peak stage where the stress dropped until residual strength is reached.

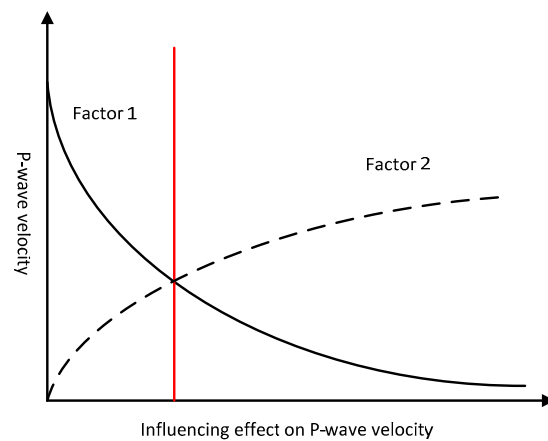


Figure 6. In the illustration of the two factors on P-wave velocity, factor 1 is negative and factor 2 is positive.

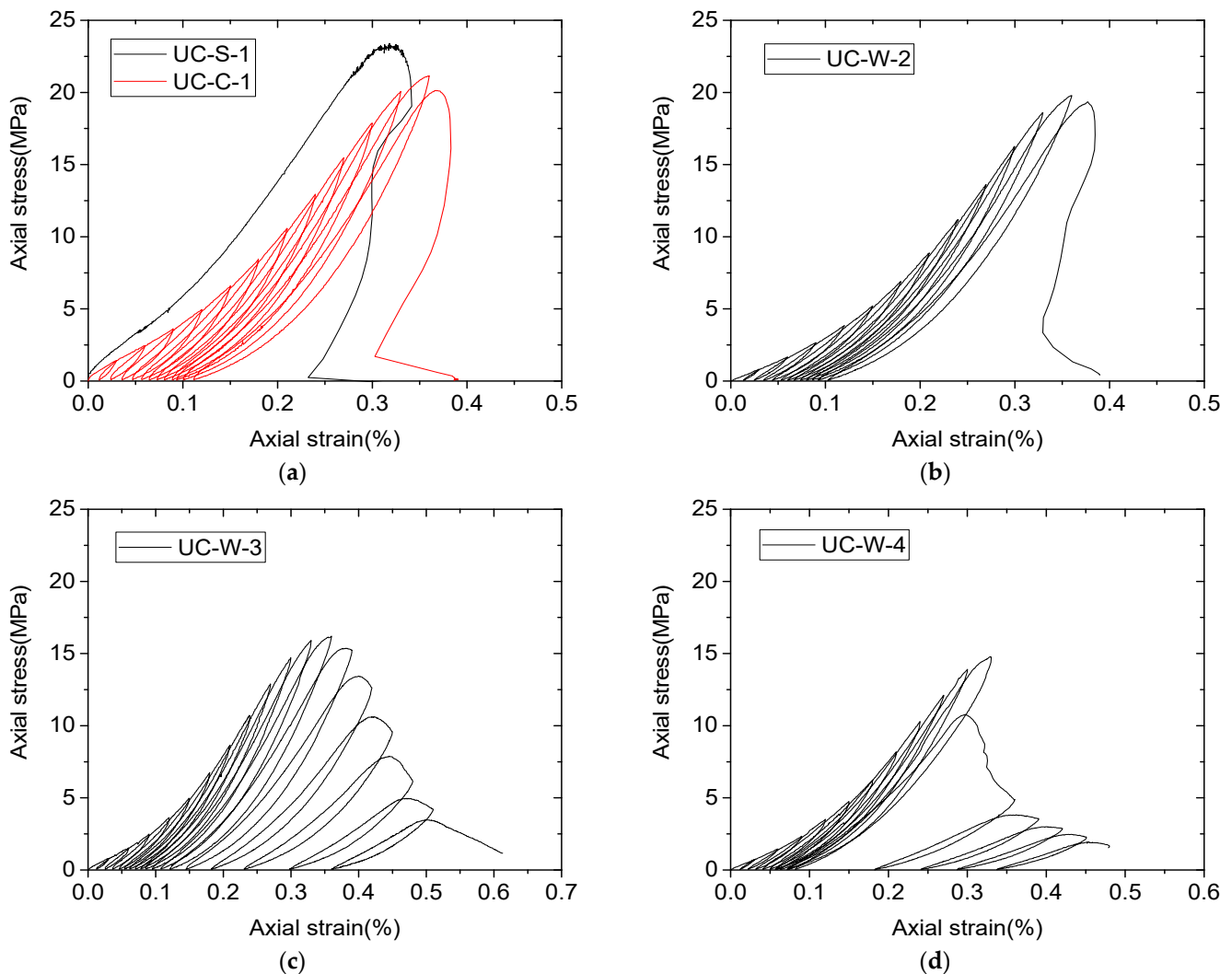


Figure 7. Stress-strain curves of the Beizao sandstone with different water content: (a) $w = 0$, (b) $w = 2.992\%$, (c) $w = 3.493\%$, and (d) $w = 3.936\%$.

As a complex geological material, rocks contain microcracks, pores, or other flaws, which lead to the formation of a hysteresis loop per cycle when rocks are subjected to cyclic loading (see Figure 7). It should be noted that even after the peak stress, the stress-strain curves changed from class II behavior (UC-S-1, UC-C-1, UC-W-2) to class I behavior

(UC-W-3 and UC-W-4), which has been discussed in the earlier studies [36,37]. It indicates that with increasing the water content, the failure of sandstone specimens' changes from unstable to stable.

Figure 8 shows that decrease in uniaxial compressive strength correlated with increasing the water content. In our study, compared with UC-C-1, whose water content was zero, the UCS of UC-W-2, UC-W-3, and UC-W-3 decreased by 6.51%, 23.4%, and 30.1%, respectively.

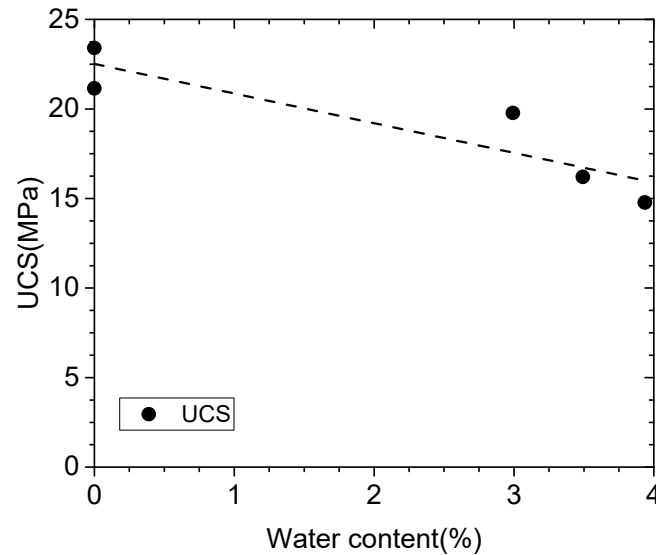


Figure 8. Variation of UCS in Beizao sandstone specimens with various water content.

4. Discussion

Figure 9 shows the diagram of one cycle of UC-C-1. In Figure 9, ϵ_r^i is the residual strain which cannot recover during the unloading process and is mainly caused by the cracks of rocks. ϵ_e^i represents elastic strain, the recoverable deformation when the stress is unloaded. The loading Young's modulus (E_L^i) and unloading Young's modulus (E_U^i) is defined as the slope of the section from the 30% to 80% peak stress in the stress-strain curve at each loading and unloading cycle. σ_u^i is the unloading stress per cycle.

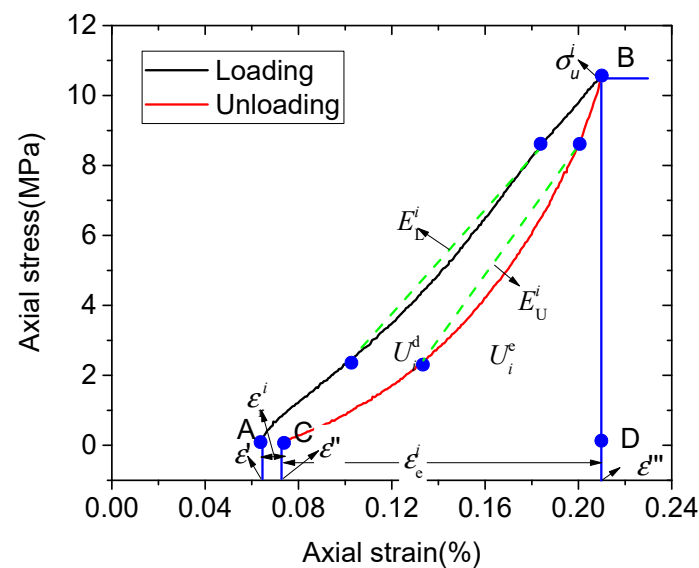


Figure 9. Diagram of elastic deformation, residual deformation, elastic modulus elastic energy, and dissipated energy under cyclic loading-unloading condition.

The failure process of rocks has four stages: crack closure, crack initiation, crack growth and crack coalescence. All the stages require energy. For example, the formation of new fractures and the friction among the fractures will dissipate energy. Cyclic loading tests are an effective way to identify the energy evolution characteristics (elastic energy and dissipated energy) of rocks [25,38]. In Figure 9, the elastic energy density (U_i^e) and dissipated energy (U_i^d) density are presented. The area (ABD) under the loading stress-strain curve is the input energy density (U_i^c), which is the total energy exerted by the test machine on the sandstone specimen. The area (BCD) under the unloading stress-strain curve is U_i^e , which is the energy stored in the specimen. The area (ABC) between the loading and unloading stress-strain curve is U_i^d which is the energy that dissipated by crack evolution. From Figure 9, we can see the relationship between U_i^c , U_i^d , and U_i^e .

$$\begin{cases} U_i^c = \int_{\epsilon'}^{\epsilon''} \sigma_1 d\epsilon_1 \\ U_i^e = \int_{\epsilon''}^{\epsilon'''} \sigma_1 d\epsilon_1 \\ U_i^d = U_i^c - U_i^e \end{cases} \quad (4)$$

where ϵ' , ϵ'' , and ϵ''' are the corresponding strain of points A, C, and B in Figure 9.

4.1. Young's Modulus

Figure 10 shows the evolution of Young's modulus of the samples with the increase in number of cycles. One can observe in Figure 10a that with the increase of the number of cycles, E_L^i increased until 10 (UC-W-2, UC-W-3, and UC-W-4) and 11 (UC-C-1) cycles. Then, E_L^i started decreasing with the number of cycles. The increase of E_L^i is because of the closure of pre-existing cracks in the samples. With continuous loading and unloading, the sandstone specimens sustained damage that led to the decrease of E_L^i . At the post-peak stage, E_L^i gradually decreased with the number of cycles, indicating that more cracks were generated.

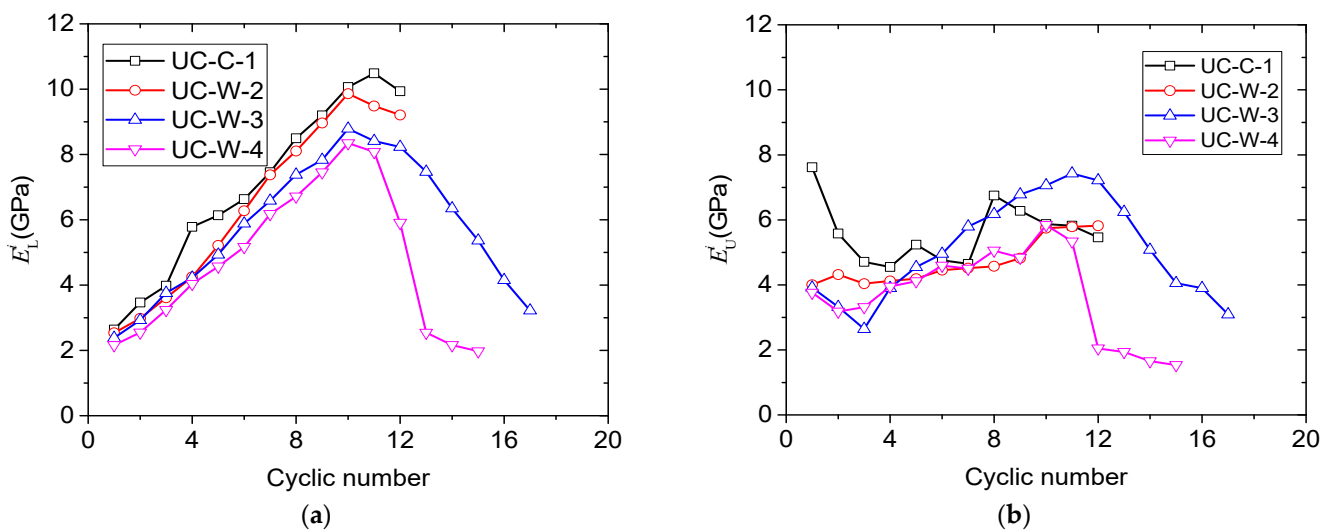


Figure 10. Variations of the loading Young's modulus and unloading Young's modulus with number of cycles: (a) relationship between loading Young's modulus and cyclic number and (b) relationship between unloading Young's modulus and number of cycles.

Figure 10b shows the evolution of E_U^i with the number of cycles. It can be observed from Figure 10b that E_U^i initially decreased, then increased, and finally decreased again with increasing the number of cycles, which seems similar to an "S" shape.

Furthermore, Figure 10a illustrates the effects of water on the sandstone specimens. At the same number of cycles, the loading Young's modulus of the sandstone specimens with less water content is lower than that with more water content. With continuous cyclic loading-unloading compression, damage to the sandstone specimens can occur, i.e.,

Young's modulus decreases. At 12 cycles, three sandstone specimens (UC-C-1, UC-W-2, and UC-W-3) reached their peak strength, and UC-W-4 reached its peak strength at 11 cycles. It should be noted that E_L^i started decreasing at 11 (UC-C-1) and 10 (UC-W-2, UC-W-3, and UC-W-4) cycles after reaching its peak, which indicated that the presence of water can weaken the elasticity of rocks.

4.2. Unloading Stress

Figure 11 provides the variations of unloading stress and its increments at each cycle of the sandstone specimens under cyclic loading compression with different water content. From Figure 11a, it can be seen that with the increase in the number of cycles, the unloading stress of the sandstone also gradually increased before peak strength. Furthermore, at each cycle, the unloading stress of the sandstone with less water content was larger than it with more water content. After peak strength, the unloading stress decreased with the number of cycles.

Figure 11b illustrates the relationship between the increment of unloading stress and the number of cycles. The increment of unloading stress ($\Delta\sigma_u^i$) can be calculated by the following equation:

$$\Delta\sigma_u^i = \sigma_u^{i+1} - \sigma_u^i \quad (5)$$

where i is the number of cycles.

In our cyclic loading tests, the interval strain between each unloading stress was 0.03% (Section 2.3). The evolution of $\Delta\sigma_u^i$ is an indication of the change in characteristics of damage during the cyclic loading process. One can observe from Figure 11b that, initially, $\Delta\sigma_u^i$ increased slightly and then decreased with the number of cycles. The turning points were 9 (UC-C-1), 10 (UC-W-2), 9 (UC-W-3), and 8 (UC-W-4) cycles, which shows that with increasing the water content, the turning point concerning the number of cycles had a decreasing trend. After the peak strength, $\Delta\sigma_u^i$ became negative and had a slight increasing trend at the last three cycles. The sharp decrease of $\Delta\sigma_u^i$ in UC-W-4 was due to the brittle failure of the sandstone specimen, which can be seen in Figure 7d.

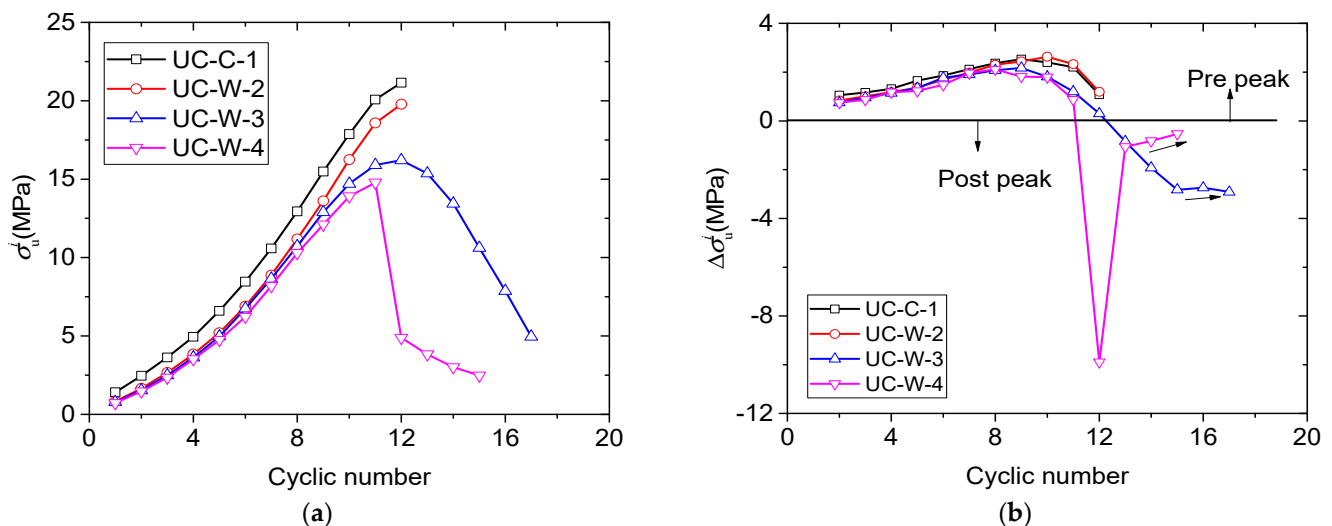


Figure 11. Variations of the unloading stress and increment of unloading stress with number of cycles: (a) relationship between unloading stress and number of cycles and (b) relationship between the increment of unloading stress and number of cycles.

4.3. Residual Strain and Elastic Strain

Figure 12 shows the relationship between the number of cycles and the strains for the sandstone specimens under cyclic loading compression with different water content. From Figure 12a, we can see that with the increase in the number of cycles, the residual strain for all sandstone specimens, at first, slightly decreased, and then increased at 10 (UC-C-1),

11 (UC-W-2), 10 (UC-W-3) and 7 (UC-W-4) cycles. The decrease in residual strain was due to the closure of pre-existing cracks of the sandstone specimens under the effects of cyclic compression. Under the effects of the continuous cyclic loading, damage to the sandstone specimens occurred and some cracks were generated, and hence the residual strain increased with the number of cycles. The residual strain of UC-W-4 at 11 cycles was nearly negative and had a sharp increase at 12 cycles, which indicated the brittle failure of UC-W-4 at 11 cycles.

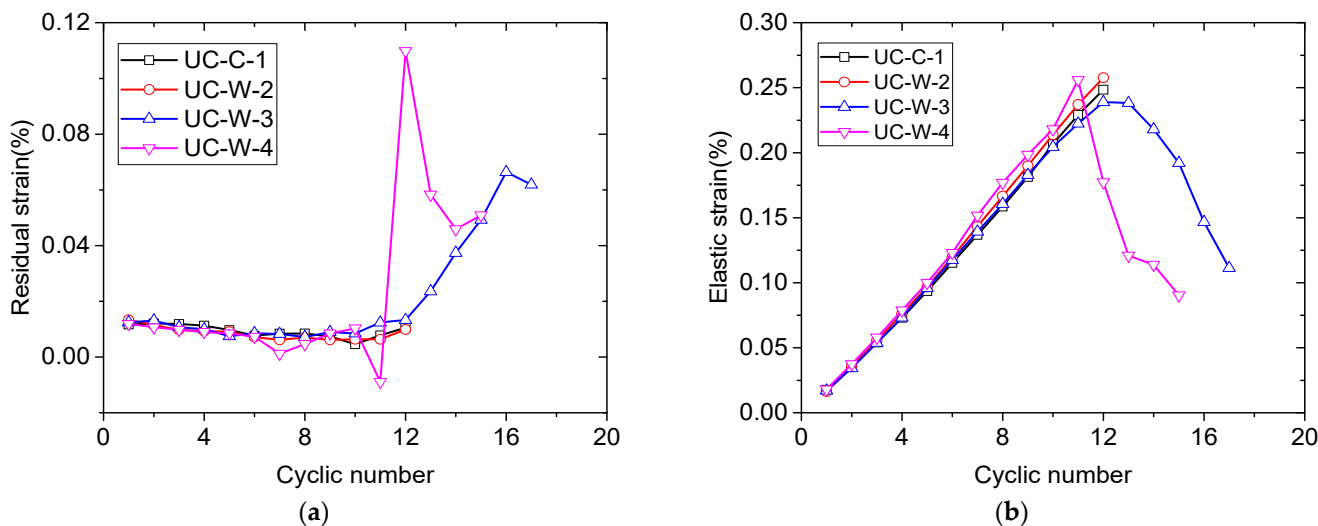


Figure 12. Variations of the residual strain and elastic strain with number of cycles: (a) relationship between residual strain and cycle number and (b) relationship between elastic strain and number of cycles.

Figure 12b shows the relationship between the number of cycles and elastic strain for the sandstone with differing water content that is unlike those of the residual strain of the sandstone shown in Figure 12a. It can be seen from Figure 12b that with the increase in number of cycles, the elastic strain for the sandstone specimens at first increased and then decreased, and the elastic strain at each cycle differs for the various water contents.

Figure 13 illustrates the relationship between the strains and unloading stress of the sandstone specimens under cyclic loading compression with different water contents. It can be seen from Figure 13a that with the increase in unloading stress, the residual deformation of the sandstone had a slightly decreasing trend and then increased with the unloading stress before peak strength. Furthermore, after peak strength, the residual strain increased with decreasing unloading stress. Figure 13b shows the effect of unloading stress on the elastic deformation of the sandstone. One can observe from Figure 13b that, with the increase in unloading stress, the elastic strain gradually increased before peak strength, and after peak strength, the elastic strain decreased with unloading stress.

4.4. Energy Evolution Characteristics

According to Figure 9, the input, elastic, and dissipated energy densities can be calculated. Figure 14 shows relationships between the input, elastic, and dissipated energy densities and unloading stress of the sandstone specimens with different water content. The curves for all three energy densities showed a similar trend with unloading stress before peak strength. With the increase in unloading stress, the energy densities for the sandstone specimens nonlinearly increased. Furthermore, the curves for the relationship between energy densities and unloading stress almost overlapped with the lower unloading stress, i.e., the curves of input energy density with unloading stress shown in Figure 14a overlapped with other curves approximately at 6 MPa and then separated from other curves due to the effects of water.

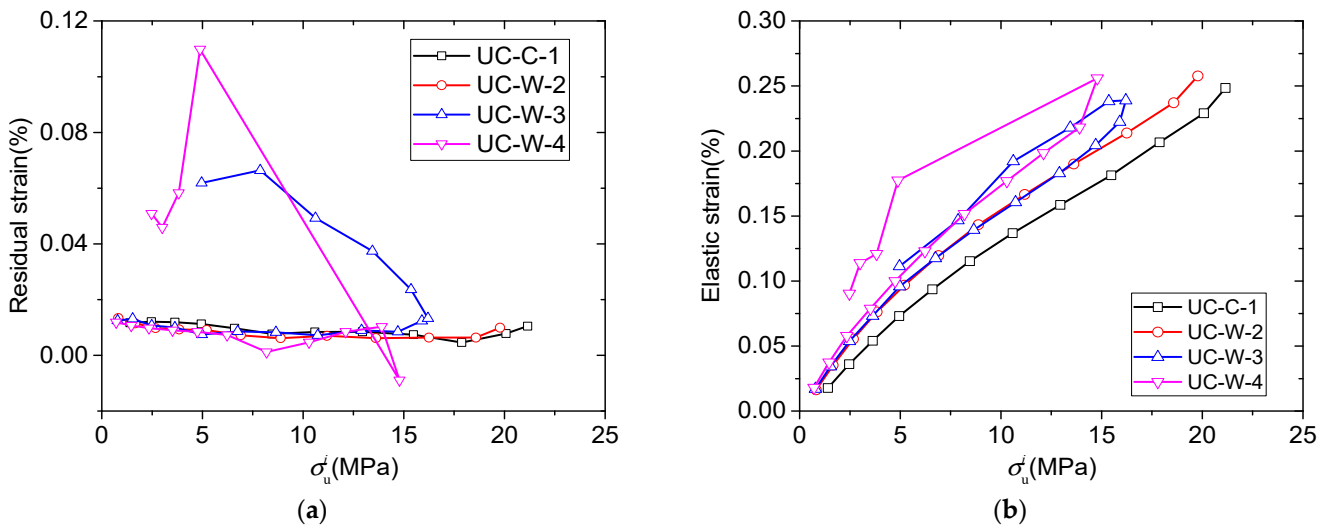


Figure 13. (a) Relationship between unloading stress and residual strain, and the (b) relationship between unloading stress and elastic strain.

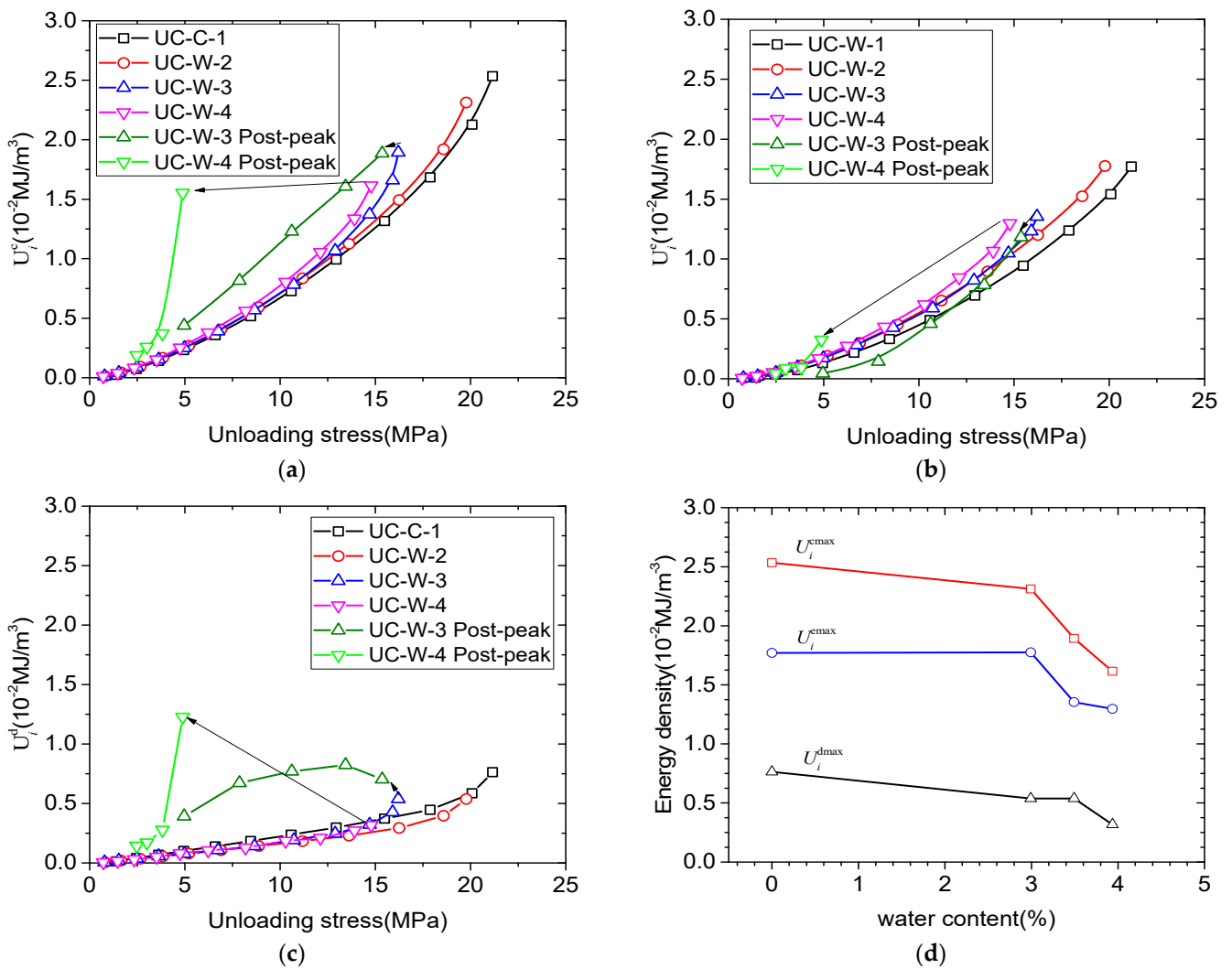


Figure 14. Relationship between energy density and unloading stress: (a) input energy density, (b) elastic energy density, (c) dissipated energy density, and (d) relationship between peak energy density and water content.

At the same unloading stress, i.e., 15 MPa, both input energy densities and elastic energy densities increased with the increase in water content. However, the dissipated energy densities did not show an obvious relationship with water content. After the peak strength, at the same unloading stress, the input energy densities and dissipated energy densities of UC-W-3 and UC-W-4 (Figure 14a,c) were larger than those before peak strength. This is because, after peak strength, the main fractures were generated and the friction among the fractures consumed more energy than during the pre-peak stage in the same stress condition. However, the elastic energy densities after the peak strength were less than those before the peak strength. Figure 14d shows that the peak input energy density (U_i^{cmax}), peak elastic energy density (U_i^{emax}), and peak dissipated energy density (U_i^{dmax}) decrease with the increase in water content.

Figure 15 shows the plot of the elastic energy ratio and dissipated energy ratio of the sandstone specimens against number of cycles. It can be observed from Figure 15a that the elastic energy ratio increased with the number of cycles, and the increase rate gradually decreased. Before peak strength, the elastic energy ratio decreased with the number of cycles, e.g., the elastic energy ratio of UC-C-1 decreased at 10 cycles. Compared with the elastic energy ratio, the evolution of the dissipated energy ratio showed the opposite trend. After peak strength, the dissipated energy ratio increased with the increase in number of cycles.

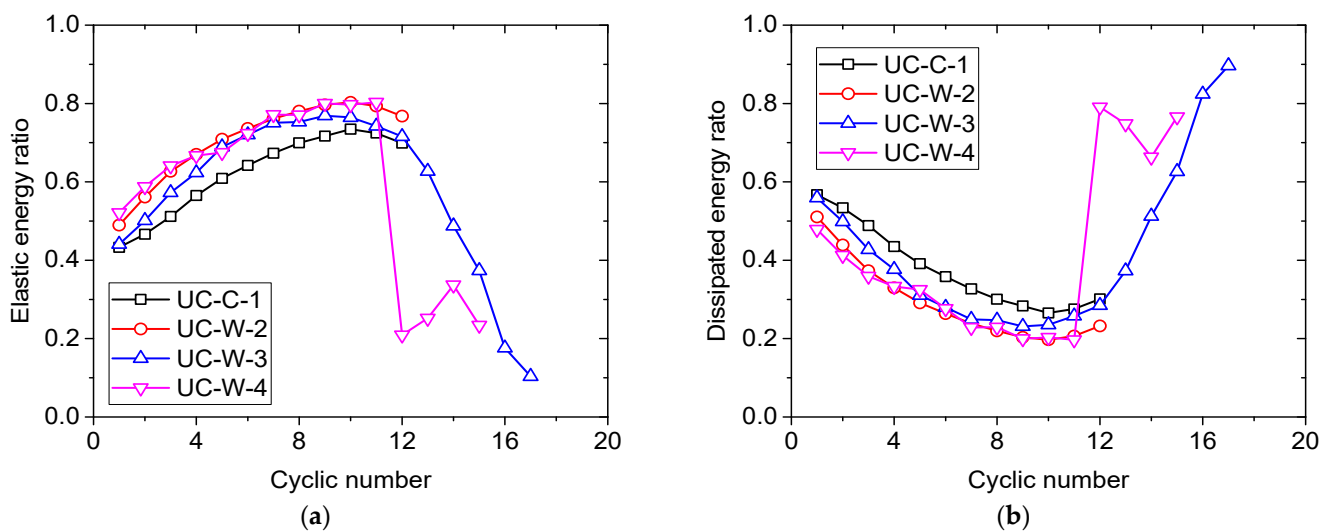


Figure 15. (a) Variation of elastic energy ratio with number of cycles, and (b) variation of dissipated energy ratio with number of cycles.

Figure 16 shows the relationship between unloading stress and energy ratio of the sandstone specimens under cyclic loading compression with various water content. From Figure 16a, it can be seen that with the increase in unloading stress, the elastic energy ratio of sandstone gradually increased, and then decreased. In contrast, one can observe from Figure 16b that the dissipated energy ratio decreased and then increased before peak strength due to the crack evolution of the sandstone specimens. After peak strength, the dissipated energy ratio sharply increased. The closure of the large amount of the original cracks in the rock consumes energy. Under cyclic loading, the original cracks were gradually consolidated, and the dissipated energy ratio gradually decreased, as does the decreasing rate. It should be noted that the dissipated energy ratio is larger than the elastic energy ratio after peak strength because of the crack growth.

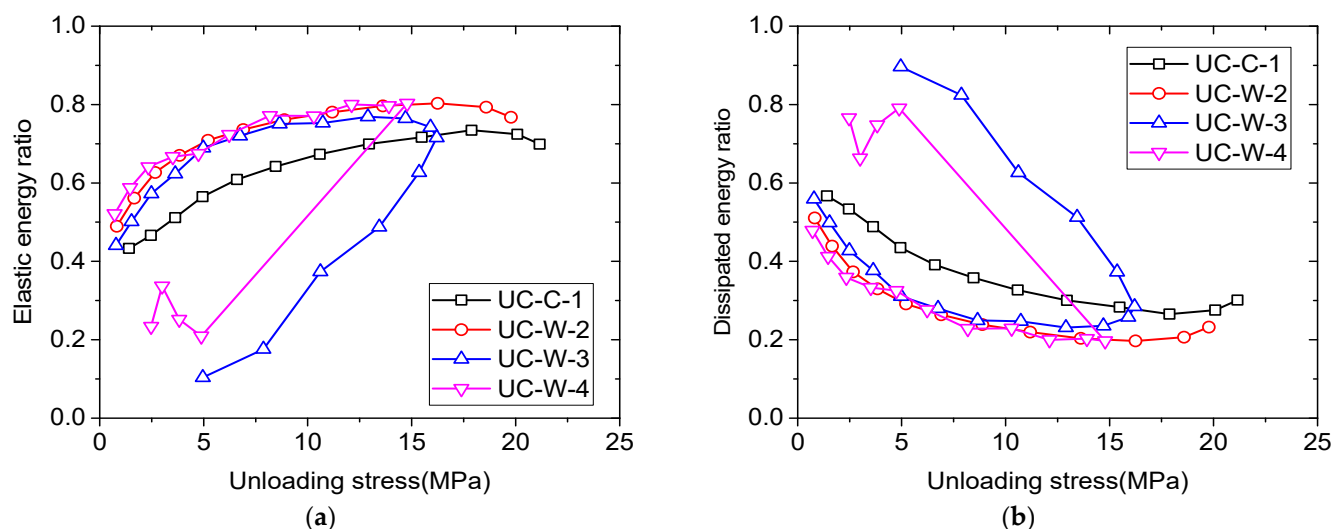


Figure 16. (a) Relationship between elastic energy ratio and unloading stress, and (b) the relationship between dissipated energy ratio and unloading stress.

Previous studies have shown that during the process from the elastic stage, plastic stage to the failure stage in the stress-strain curve, there is always energy exchange with the outside world, and energy is constantly released to the outside world to maintain dynamic balance [39]. Through the experimental results of sandstone with different water content under cyclic loading, the water can weaken the sandstone underneath the Bohai Sea. In addition, with the increase in water content, smaller energy input can cause the failure of sandstone. Therefore, the water content of the sandstone in case of roof fall, water inrush, or other hazards must be carefully monitored.

5. Conclusions

This study explored the effect of water on mechanical properties and energy evolution characteristics of Beizao sandstone using a series of uniaxial cyclic loading experiments. Based on the experimental results, the main conclusions drawn from the investigation are given below.

- (1) With the increase in immersion time, mass difference, Δm , and water content, w , the increase and increase rates decreased with immersion time. The trend of P-wave velocity at first decreased and then increased.
- (2) The presence of water can weaken the loading Young's modulus, peak strength, unloading stress, and post-peak stage of stress-strain curves of the sandstone specimens. The residual strain firstly decreased with the number of cycles because of the closure of pre-existing cracks, and then it increased with the number of cycles. Elastic strain showed an increasing trend with the increase in the number of cycles before peak strength.
- (3) The input energy density of the sandstone specimens with more water content was larger than those with less water content at the same unloading stress. The peak energy densities showed a decreasing trend with the increase in water content. At the same number of cycles and unloading stress, the elastic energy ratio with less water content was lower than that with more water content. In addition, the dissipated energy ratio showed the opposite trend.

Author Contributions: Conceptualization, Y.C. and R.D.; methodology, Y.C.; software, E.B.; validation, Y.C., G.Z. and B.G.; formal analysis, Y.C.; investigation, Y.C.; resources, Y.C.; data curation, G.Z.; writing—original draft preparation, Y.C.; writing—review and editing, Y.C. and B.G.; visualization, R.D.; supervision, Y.C.; project administration, Y.C.; funding acquisition, Y.C. All authors have read and agreed to the published version of the manuscript.

Funding: This research was funded by National Natural Science Foundation of China (grant number 51904092), the Fundamental Research Funds for the Universities of Henan Province (grant number NSFRF210454), the Young Backbone Teachers Funding Program of Henan Polytechnic University (grant number 2022XQG-01) and Doctor Fund supported by Henan Polytechnic University (B2019-21).

Data Availability Statement: Not applicable.

Conflicts of Interest: The authors declare no conflict of interest.

References

1. Zuo, J.; Peng, S.; Li, Y.; Chen, Z.; Xie, H. Investigation of karst collapse based on 3-D seismic technique and DDA method at Xieqiao coal mine, China. *Int. J. Coal Geol.* **2009**, *78*, 276–287. [\[CrossRef\]](#)
2. Zhu, W.; Wei, C. Numerical simulation on mining-induced water inrushes related to geologic structures using a damage-based hydromechanical model. *Environ. Earth Sci.* **2011**, *62*, 43–54. [\[CrossRef\]](#)
3. He, X.; Song, L. Status and future tasks of coal mining safety in China. *Saf. Sci.* **2012**, *50*, 894–898. [\[CrossRef\]](#)
4. Li, X.; Li, Q.; Hu, Y.; Teng, L.; Yang, S. Evolution characteristics of mining fissures in overlying strata of stope after converting from open-pit to underground. *Arab. J. Geosci.* **2021**, *14*, 2795. [\[CrossRef\]](#)
5. Guo, B.; Cheng, T.; Wang, L.; Luo, T.; Yang, X. Physical simulation of water inrush through the mine floor from a confined aquifer. *Mine Water Environ.* **2018**, *37*, 577–585. [\[CrossRef\]](#)
6. Yang, S.; Jing, H.; Wang, S. Experimental investigation on the strength, deformability, failure behavior and acoustic emission locations of red sandstone under triaxial compression. *Rock Mech. Rock Eng.* **2012**, *45*, 583–606. [\[CrossRef\]](#)
7. Xu, N.; Dai, F.; Li, B.; Zhu, Y.; Zhao, T.; Yang, D. Comprehensive evaluation of excavation-damaged zones in the deep underground caverns of the Houziyan hydropower station, Southwest China. *Bull. Eng. Geol. Environ.* **2017**, *76*, 275–293. [\[CrossRef\]](#)
8. Sirdesai, N.; Mahanta, B.; Ranjith, P.; Singh, T. Effects of thermal treatment on physico-morphological properties of Indian fine-grained sandstone. *Bull. Eng. Geol. Environ.* **2017**, *78*, 883–897. [\[CrossRef\]](#)
9. Li, X.; Peng, J.; Xie, Y.; Li, Q.; Zhou, T.; Wang, J.; Zheng, W. Influence of high-temperature treatment on strength and failure behaviors of a quartz-rich sandstone under true triaxial condition. *Lithosphere* **2022**, *2022*, 3086647. [\[CrossRef\]](#)
10. Gatelier, N.; Pellet, F.; Loret, B. Mechanical damage of an anisotropic porous rock in cyclic triaxial tests. *Int. J. Rock Mech. Min. Sci.* **2002**, *39*, 335–354. [\[CrossRef\]](#)
11. Bagde, M.; Petroš, V. Waveform effect on fatigue properties of intact sandstone in uniaxial cyclical loading. *Rock Mech. Rock Eng.* **2005**, *38*, 169–196. [\[CrossRef\]](#)
12. Yang, S.; Jing, H. Strength failure and crack coalescence behavior of brittle sandstone samples containing a single fissure under uniaxial compression. *Int. J. Fract.* **2011**, *168*, 227–250. [\[CrossRef\]](#)
13. Kong, B.; Wang, E.; Li, Z.; Li, Z.; Wang, X.; Niu, X.; Kong, X. Acoustic emission signals frequency-amplitude characteristics of sandstone after thermal treated under uniaxial compression. *J. Appl. Geophys.* **2017**, *136*, 190–197. [\[CrossRef\]](#)
14. Ray, S.; Sarkar, M.; Singh, T. Effect of cyclic loading and strain rate on the mechanical behaviour of sandstone. *Int. J. Rock Mech. Min. Sci.* **1999**, *36*, 543–549. [\[CrossRef\]](#)
15. Fuenkajorn, K.; Phueakphum, D. Effects of cyclic loading on mechanical properties of MahaSarakhm salt. *Eng. Geol.* **2010**, *112*, 43–52. [\[CrossRef\]](#)
16. Baud, P.; Zhu, W.; Wong, T. Failure mode and weakening effect of water on sandstone. *J. Geophys. Res.* **2000**, *105*, 16371–16389. [\[CrossRef\]](#)
17. Vászárhelyi, B.; Ván, P. Influence of water content on the strength of rock. *Eng. Geol.* **2006**, *84*, 70–74. [\[CrossRef\]](#)
18. Erguler, Z.; Ulusay, R. Water-induced variations in mechanical properties of clay-bearing rocks. *Int. J. Rock Mech. Min. Sci.* **2009**, *46*, 355–370. [\[CrossRef\]](#)
19. Li, D.; Wong, L.; Liu, G.; Zhang, X. Influence of water content and anisotropy on the strength and deformability of low porosity meta-sedimentary rocks under triaxial compression. *Eng. Geol.* **2012**, *126*, 46–66. [\[CrossRef\]](#)
20. Fairhurst, C.; Hudson, J. Draft ISRM suggested method for the complete stress-strain curve for intact rock in uniaxial compression. *Int. J. Rock Mech. Min. Sci. Geomech. Abstr.* **1999**, *36*, 279–289. [\[CrossRef\]](#)
21. Chen, Y.; Zuo, J.; Guo, B.; Guo, W. Effect of cyclic loading on mechanical and ultrasonic properties of granite from Maluanshan Tunne. *B Eng. Geol. Environ.* **2020**, *79*, 299–311. [\[CrossRef\]](#)
22. Chen, Y.; Guo, W.; Zuo, J.; Heng, S.; Dou, R. Effect of triaxial loading and unloading on crack propagation and damage behaviors of sandstone: An experimental study. *Rock Mech. Rock Eng.* **2021**, *54*, 6077–6090. [\[CrossRef\]](#)
23. Bieniawski, Z. Time-dependent behaviour of fractured rock. *Rock Mech. Rock Eng.* **1970**, *2*, 123–137. [\[CrossRef\]](#)
24. Chong, K.; Hoyt, P.; Smith, J.; Paulsen, B. Effects of strain rate on oil shale fracturing. *Int. J. Rock Mech. Min. Sci. Geomech. Abstr.* **1980**, *17*, 35–43. [\[CrossRef\]](#)
25. Meng, Q.; Zhang, M.; Han, L.; Pu, H.; Nie, T. Effects of acoustic emission and energy evolution of rock specimens under the uniaxial cyclic loading and unloading compression. *Rock Mech. Rock Eng.* **2016**, *49*, 3873–3886. [\[CrossRef\]](#)
26. Nur, A.; Simmons, G. The effect of saturation on velocity in low porosity rocks. *Earth Planet. Sci. Lett.* **1969**, *7*, 183–193. [\[CrossRef\]](#)
27. Wang, C.; Lin, W.; Wenk, H. The effects of water and pressure on velocities of elastic waves in a foliated rock. *J. Geophys. Res.* **1975**, *80*, 1065–1069. [\[CrossRef\]](#)

28. King, M.; Marsden, J.; Dennis, J. Biot dispersion for P-and S-wave velocities in partially and fully saturated sandstones. *Geophys. Prospect.* **2000**, *48*, 1075–1089. [[CrossRef](#)]
29. Kahraman, S. The correlations between the saturated and dry P-wave velocity of rocks. *Ultrasonics* **2007**, *46*, 341–348. [[CrossRef](#)]
30. Karakul, H.; Ulusay, R. Empirical correlations for predicting strength properties of rocks from P-wave velocity under different degrees of saturation. *Rock Mech. Rock Eng.* **2013**, *46*, 981–999. [[CrossRef](#)]
31. Martin, C.; Chandler, N. The progressive fracture of Lac du Bonnet granite. *Int. J. Rock Mech. Min. Sci. Geomech. Abstr.* **1994**, *31*, 643–659. [[CrossRef](#)]
32. Eberhardt, E.; Stead, D.; Stimpson, B.; Read, R. Identifying crack initiation and propagation thresholds in brittle rock. *Can. Geotech. J.* **1998**, *35*, 222–233. [[CrossRef](#)]
33. Cai, M.; Kaiser, P.; Tasaka, Y.; Maejima, T.; Morioka, H.; Minami, M. Generalized crack initiation and crack damage stress thresholds of brittle rock masses near underground excavations. *Int. J. Rock Mech. Min. Sci.* **2004**, *41*, 833–847. [[CrossRef](#)]
34. Tkalich, D.; Fourmeau, M.; Kane, A.; Li, C.; Cailletaud, G. Experimental and numerical study of Kuru granite under confined compression and indentation. *Int. J. Rock. Mech. Min. Sci.* **2016**, *87*, 55–68. [[CrossRef](#)]
35. Chen, Y.; Wei, K.; Liu, W.; Hu, S.; Hu, R.; Zhou, C. Experimental characterization and micromechanical modelling of anisotropic slates. *Rock Mech. Rock Eng.* **2016**, *49*, 3541–3557. [[CrossRef](#)]
36. Wawersik, W.; Fairhurst, C. Study of brittle rock fracture in laboratory compression experiments. *Int. J. Rock Mech. Min. Sci. Geomech. Abstr.* **1970**, *7*, 561–575. [[CrossRef](#)]
37. Hudson, J.; Crouch, S.; Fairhurst, C. Soft, stiff and servo-controlled testing machines: A review with reference to rock failure. *Eng. Geol.* **1972**, *6*, 155–189. [[CrossRef](#)]
38. Huang, D.; Li, Y. Conversion of strain energy in triaxial unloading tests on marble. *Int. J. Rock Mech. Min. Sci.* **2014**, *66*, 160–168. [[CrossRef](#)]
39. Dai, B.; Luo, X.; Shan, Q.; Chen, Y.; Liu, Y. Analysis on damage characteristics and energy dissipation of rock with a single hole under cyclic impact loads. *China Saf. Sci. J.* **2020**, *30*, 69–77. [[CrossRef](#)]